

Fubini-Study metric as a tool to classify the topological properties of flat band electronic states: the case of an atomic chain with $s - p$ orbitals.

Abdiel Espinosa-Champo and Gerardo G. Naumis.*

*Depto. de Sistemas Complejos, Instituto de Física,
Universidad Nacional Autónoma de México (UNAM)*

Apdo. Postal 20-364, 01000, CDMX, Mexico.

(Dated: March 23, 2023)

The topological properties of flat band states of a one-electron Hamiltonian describing a chain of atoms with $s - p$ orbitals are explored. This model is mapped onto a Kitaev-Creutz type model providing a useful framework to understand the topology through a non-trivial winding number and the geometry introduced by the *Fubini-Study* (*FS*) metric. This metric allows us to distinguish between pure states of systems with the same topology and thus provides a suitable tool to obtain the fingerprint of flat bands. Moreover, it provides an appealing geometrical picture to describe flat bands, as it can be associated with a local conformal transformation over circles in a complex plane. In addition, the presented model allows to relate the topology with the formation of Compact Localized States (CLS) and Bogoliubov-like modes. The presented model is equivalent to two interacting SSH chains under a change of basis and thus provides the most simple generalization of the SSH model able to present flat bands. Experimentally, the proposed system can be realized with boron, gallium, and tellurium.

I. INTRODUCTION.

A flat band indicates a band structure with constant energy independent of the crystal momentum. The quenched kinetic energy in a flat band suppresses wave transport; i.e., the wave group velocity $\nabla_{\mathbf{k}} E(\mathbf{k})$ vanishes. This results in a strong sensitivity to perturbations, and any perturbation can set a new dominant energy scale for the flat band states and qualitatively change their transport properties [1].

Due to this, flat band systems have been considered intriguing in various research areas [2–9]. In condensed matter, flat bands are considered ideal to study many-body phenomena such as ferromagnetism [10, 11], superconductivity [12, 13], and Wigner crystal formation [14, 15] because the kinetic energy of the carriers in the flat band is quenched and dominated by the electron-electron interaction. In bosonic systems such as photonic crystals, the realization of slow light via a flat band has received great attention because it can be applied to enhance the light-matter interaction [16, 17].

Usually, perfectly flat bands require either fine-tuning of system parameters or protection by a lattice symmetry. In addition, they are not stable against generic perturbations, which typically induce nonzero dispersion. For this reason, some authors broaden the definition of flat bands to include partially flat bands that have vanishing dispersion only along particular directions or in the vicinity of special Brillouin zone points [18–20] and also define the flatness ratio $F = \Delta/W$, in terms of the bandwidth, W , and the energy gap Δ , to quantify how good a flat band model is [18].

Historically, the study of flat band models originates with Sutherland’s observation [21] of a flat band and

its ‘strictly localized states’ in the dice lattice. Then came Lieb’s paper on the Hubbard model, which proved that certain bipartite lattices with chiral flat bands exhibit ferromagnetism at half-filling [22]. Shortly afterward, Mielke and Tasaki independently generalized this idea to examples of flat band ferromagnetism, occurring when the lowest single-particle energy band is flat [10, 23, 24]. Mielke’s construction of flat band lattices was based on line graphs, which are formed by promoting the links of an ordinary lattice into sites. On the other hand, the flat bands in Tasaki’s ‘decorated’ lattices emerge due to competition between fine-tuned nearest- and next-nearest neighbor hopping.

In 1993, Shima and Aoki introduced a class of superlattices exhibiting symmetry-protected chiral flat bands [25], and he was the first to introduce the name ‘compact localized state’ (CLS) for flat band eigenmodes constructed as a superposition of the degenerate Bloch waves [26].

Although the interest in flat bands systems came up long ago, they have received renewed interest since the discovery of unconventional superconductivity in graphene [12]; mainly with a special focus on topological flat-band models [18], due that the proposed topological flat-bands is just like the counterpart of the Landau Levels (LL), characterized by a Chern number [27, 28]. It has been shown by numerical simulations that flat bands support Quantum Hall-like states, exhibiting not only the integer Quantum Hall (QH) effects but also the Fractional Quantum Hall (FQH) effects [29–31] and the existence of electronic Fractional Chern states analogs of the Laughlin state [8, 9, 29, 32].

Crucially, these works required the study of the topological properties of flat band states. However, the Chern number is not enough to fully characterize the properties of such quantum phases. Therefore, the *FS* metric has been added as a tool to distinguish between pure

* naumis@fisica.unam.mx

states of systems with the same topology; in particular, to distinguish the formation of flat bands [33–36]. Despite this, no simple models are available to understand how all these tools work. In this work, we propose a 1D tight-binding model that exhibits a topological transition with a nontrivial winding number, and its *FS* metric allows us to identify flatness regions reliably. The model is also strongly motivated by recent works indicating that chains of elements such as boron [37], gallium [38], and tellurium [39, 40] are promising candidates for the experimental realization of the proposed model. Moreover, the model under certain transformations is also very similar to two interacting SSH chains giving the most simple generalization to it. Furthermore, the proposed model would be useful in order to search for a soluble flat-band electron-electron interaction model.

This work is organized as follows. In Sec. II, we introduce the atomic chain model and the effective hamiltonian, which then is mapped into a bipartite Kitaev-Creutz type chain. In Sec. III we discuss the formation of Bogoliubov-like modes and the existence of a certain regime with flat bands in which CLS exists. They are characterized by analogous to Landau Level relations. Furthermore, we show the non-trivial topology phase transition and how the geometry, characterized by the *FS* metric, allows us to distinguish between flat band regimes from other topological systems. Finally, we summarize and conclude in Sec. IV.

II. HAMILTONIAN MODEL.

As a model, we will consider an atomic chain with $s-p$ orbitals (see Fig. 1). Assuming a tight-binding model with only first-neighbors interaction, the hamiltonian is given by

$$\begin{aligned} \hat{\mathcal{H}} = & \sum_{\mathbf{r}_n} (\varepsilon_s(\mathbf{r}_n) c_{s,\mathbf{r}_n}^\dagger c_{s,\mathbf{r}_n} + \varepsilon_p(\mathbf{r}_n) c_{p,\mathbf{r}_n}^\dagger c_{p,\mathbf{r}_n}) \\ & + \sum_{\mathbf{r}_n} \left[t_{ss}(\mathbf{r}_n) c_{s,\mathbf{r}_{n+1}}^\dagger c_{s,\mathbf{r}_n} + t_{pp}(\mathbf{r}_n) c_{p,\mathbf{r}_{n+1}}^\dagger c_{p,\mathbf{r}_n} \right. \\ & \left. + t_{sp}(\mathbf{r}_n) c_{p,\mathbf{r}_{n+1}}^\dagger c_{s,\mathbf{r}_n} + t_{ps}(\mathbf{r}_n) c_{s,\mathbf{r}_{n+1}}^\dagger c_{p,\mathbf{r}_n} \right] + h.c. \end{aligned} \quad (1)$$

Here, the indexes α and β count over s, p orbitals, \mathbf{r}_n is the position of n -th atom, $c_{(s,p),\mathbf{r}_n}$ ($c_{(s,p),\mathbf{r}_n}^\dagger$) is the fermionic creation (annihilation) operator for the s and p orbital, $\varepsilon_{(s,p)}(\mathbf{r}_n)$ and $t_{ss}(\mathbf{r}_n)$, $t_{pp}(\mathbf{r}_n)$, $t_{sp}(\mathbf{r}_n)$, $t_{ps}(\mathbf{r}_n)$ are the on-site energy and hopping parameter to the right first neighbor, respectively. If we assume that $\varepsilon_\alpha(\mathbf{r}_n)$ and $t_{\alpha,\beta}(\mathbf{r}_n)$ are independent of the atomic position, we obtain the following set of tight-binding parameters,

$$t_{ss}, t_{pp}, t_{sp}, t_{ps} \quad (2)$$

It can be proved that from the symmetry of the p orbitals, $t_{ps} = -t_{sp}$, and t_{pp} has a sign opposite to that of t_{ss} [41].

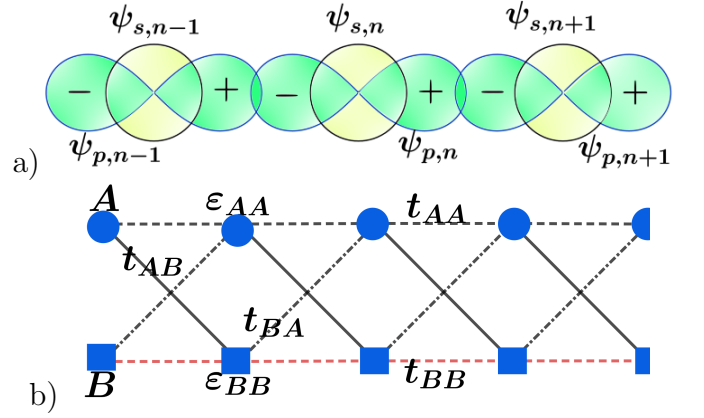


FIG. 1. a) Atomic chain with two orbitals per site. The s and p_x orbital in the n -th atom are denoted by $\psi_{s,n}$ and $\psi_{p,n}$, respectively. The near-neighbor t_{pp} hopping integral have the opposite sign to that of the near-neighbor t_{ss} hopping matrix element. The near-neighbor t_{sp} coupling alternate in sign. Inversion symmetry implies that the on-site t_{sp} coupling will vanish, just as it does in the isolated atom. b) Bipartite Kitaev-Creutz type ladder, the circles, and squares represent the sites A and B , respectively; and we can map the atomic chain onto this ladder directly, where s and p orbitals maps to A and B sites, and the hoppings follows the rules $t_{ss} \rightarrow t_{AA}$, $t_{pp} \rightarrow t_{BB}$, $t_{sp(p)} \rightarrow t_{AB(BA)}$ and $\varepsilon_{s(p)} \rightarrow \varepsilon_{A(B)}$.

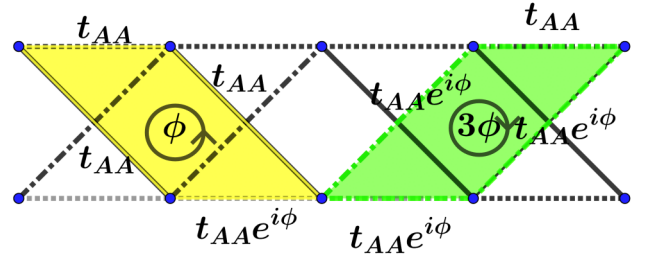


FIG. 2. Two different paths along closed plaquettes where fermions tunnel along the black links enclosing a net flux of ϕ and 3ϕ , which leads to the π -flux in Kitaev-Creutz type ladder model in Eq. (4); i.e., $\phi = \pi$.

As for each site in the chain, we have an s and p orbital, we can think of mapping the chain into a ladder, where each of these orbitals is mapped onto different sites in the ladder. As shown in Fig. 2 a), we will have different kinds of sites in the ladder, sites of type A are those obtained from the mapping of s orbitals while sites of type B come from p orbitals. The resulting ladder is equivalent to a bipartite Kitaev-Creutz type chain. Its Hamiltonian is given by,

$$\begin{aligned}
\mathcal{H} = & \sum_n (\varepsilon_A a_n^\dagger a_n + \varepsilon_B b_n^\dagger b_n) \\
& + \sum_n (t_{AA} a_{n+1}^\dagger a_n + t_{BB} b_{n+1}^\dagger b_n + h.c.) \\
& + \sum_n (t_{AB} b_{n+1}^\dagger a_n + t_{BA} a_{n+1}^\dagger b_n + h.c.)
\end{aligned} \quad (3)$$

where $a_n(a_n^\dagger)$ and $b_n(b_n^\dagger)$ are the fermionic creation (annihilation) operators for sites A and B in the n cell, respectively. We assume first that $\varepsilon_A = -\varepsilon_B = \varepsilon$, $t_{AA} = -t_{BB}$ and $t_{AB} = -t_{BA}$; then the Hamiltonian transforms to

$$\begin{aligned}
\mathcal{H} = & \varepsilon \sum_n (a_n^\dagger a_n - b_n^\dagger b_n) \\
& + t_{AA} \sum_n (a_{n+1}^\dagger a_n - b_{n+1}^\dagger b_n + h.c.) \\
& + t_{AB} \sum_n (b_{n+1}^\dagger a_n - a_{n+1}^\dagger b_n + h.c.).
\end{aligned} \quad (4)$$

Next, we perform a lattice Fourier transform using,

$$\begin{aligned}
a_k &= \frac{1}{\sqrt{N}} \sum_n a_n e^{ikx_n} \\
b_k &= \frac{1}{\sqrt{N}} \sum_n b_n e^{ikx_n}
\end{aligned} \quad (5)$$

where $x_n = nl$ and l is the lattice constant. This allows writing the Hamiltonian given by Eq. (5) in a standard Bogoliubov- de Gennes form

$$\mathcal{H} = t_{AA} \sum_k \Psi_k^\dagger \mathcal{H}(k) \Psi_k \quad (6)$$

where

$$\Psi_k = \begin{pmatrix} a_k \\ b_k \end{pmatrix}$$

and,

$$\mathcal{H}(k) = \mathbf{n}(k) \cdot \boldsymbol{\sigma} = n_x(k)\sigma_x + n_y(k)\sigma_y + n_z(k)\sigma_z; \quad (7)$$

where

$$\begin{aligned}
n_x(k) &= 0, \\
n_y(k) &= 2\lambda \sin(kl), \\
n_z(k) &= (\bar{\varepsilon} + 2 \cos(kl)),
\end{aligned} \quad (8)$$

and with the parameters defined as

$$\bar{\varepsilon} \equiv \varepsilon/t_{AA}; \lambda \equiv t_{AB}/t_{AA}. \quad (9)$$

III. GENERAL PROPERTIES AND RESULTS

In this section, we study the effective modes and topology of the Hamiltonian exposed in the previous section. First, we study how Bogoliubov and Majorana modes arise, then we study the winding number, and finally, the FS metric.

A. Bogoliubov- and Majorana-like modes

To study the effective modes, first, we will diagonalize the Hamiltonian (6) by doing a Bogoliubov transformation. We define the Bogoliubov-like modes γ_k, ρ_k as

$$\begin{aligned}
\gamma_k &\equiv u_k a_k + v_k b_k \\
\rho_k &\equiv -v_k^* a_k + u_k^* b_k
\end{aligned} \quad (10)$$

A Bogoliubov-like mode is a mixture of a fermion in sites A and B , or equivalently, a quasi-particle that hybridizes orbitals s and p . It satisfies fermionic creation and annihilation anti-commutation relations (See App. A)

$$\begin{aligned}
\{\rho_k, \rho_{k'}^\dagger\} &= \delta_{kk'}; \{\rho_k^\dagger, \rho_{k'}^\dagger\} = \{\rho_k, \rho_{k'}\} = 0 \\
\{\gamma_k, \gamma_{k'}^\dagger\} &= \delta_{kk'}; \{\gamma_k^\dagger, \gamma_{k'}^\dagger\} = \{\gamma_k, \gamma_{k'}\} = 0
\end{aligned} \quad (11)$$

where u_k and v_k are the coherent coefficients that satisfy the following properties

$$|u_k|^2 + |v_k|^2 = 1; u_{-k} = u_k; v_{-k} = -v_k \quad (12)$$

The following choice of u_k and v_k suffices the property

$$u_k = \cos\left(\frac{\omega_k}{2}\right), v_k = -i \sin\left(\frac{\omega_k}{2}\right), \quad (13)$$

where

$$\omega_k = \text{Arg}\{2i\lambda \sin(kl) + (\bar{\varepsilon} + 2 \cos(kl))\}. \quad (14)$$

Here, $\text{Arg}(z)$ refers to the principal value of $z \in \mathbb{C}$. On substituting a_k, b_k in Eq. (6), we diagonalize the Hamiltonian,

$$\begin{aligned}
\mathcal{H} &= t_{AA} \sum_k \epsilon(k) \left(\gamma_k^\dagger \gamma_k - \rho_k^\dagger \rho_k \right) \\
\epsilon(k) &= \sqrt{(\bar{\varepsilon} + 2 \cos(kl))^2 + (2\lambda \sin(kl))^2}.
\end{aligned} \quad (15)$$

In general, these Bogoliubov-like modes are related to squeezed coherent states [42] and in a similar form, they have been recently found in Twisted Bilayer Graphene (TBLG) at magic angles [43]. In the long-wavelength limit, we can expand the energy dispersion at $k = 0$ to obtain,

$$\epsilon(k) = \pm \sqrt{(\bar{\varepsilon} - \bar{\varepsilon}_c)^2 + 4\lambda^2 k^2 l^2}. \quad (16)$$

where $\bar{\varepsilon}_c = -2$. As seen in Fig. 3 there is an energy gap of size $\Delta = 2(\bar{\varepsilon} - \bar{\varepsilon}_c)$ which vanishes at the critical value $\bar{\varepsilon}_c$. At such critical $\bar{\varepsilon}_c$ the energy dispersion goes as

$$\epsilon(k) = \pm 2\lambda l |k| \quad (17)$$

We see here an emerging Dirac physics where the bulk gap closes. In such a limit, the Bogoliubov-like modes are interpreted as Majorana-like modes as we detail below.

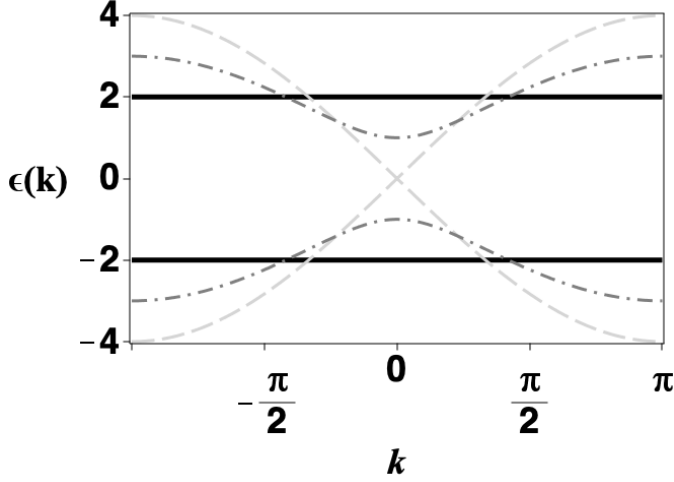


FIG. 3. The energy spectra of the Kitaev-Creutz type ladder as a function of k , for the set of values $\lambda = 1$, lattice constant l set to unity for simplicity and $\bar{\varepsilon} = -2, -1, 0$ on an ascending grayscale, respectively.

First, we consider the long-wavelength limit of the Bogoliubov-De Gennes Hamiltonian Eq. (6),

$$\mathcal{H} = t_{AA} \sum_k \Psi_k^\dagger H_D(k) \Psi_k; H_D(k) = m\sigma_z + 2\lambda k l \sigma_y \quad (18)$$

with mass in natural units, $m = (\bar{\varepsilon} - \bar{\varepsilon}_c)$. When $m \rightarrow 0$, there are two energy eigenstates with energy $E = \pm 2\lambda l |k|$. That means that the eigenstates are the equal superposition of fermions in sites A and B . They are Majorana-like modes free to propagate in the chain with speed $v = 2\lambda$.

B. Flat-band modes as Compact Localized States (CLS).

The group velocity represents the mobility of the charge carriers in the band. In the flat band, the group velocity is strictly zero for all momenta in the Brillouin zone. This implies that charge carriers are localized. The localized nature of the flat band is explained by the existence of a special localized eigenstate called the compact localized state (CLS), whose amplitude is finite only inside a finite region in real space, and exactly zero outside of it [44]. Note that the CLS is not unique, and one can have various types of the CLS by linear combinations of the smallest compact localized states centered at different positions.

1. CLS from tight-binding.

Fig. 2 shows a chain with a periodic arrangement; we see that there is a two-sublattice structure, A and B -

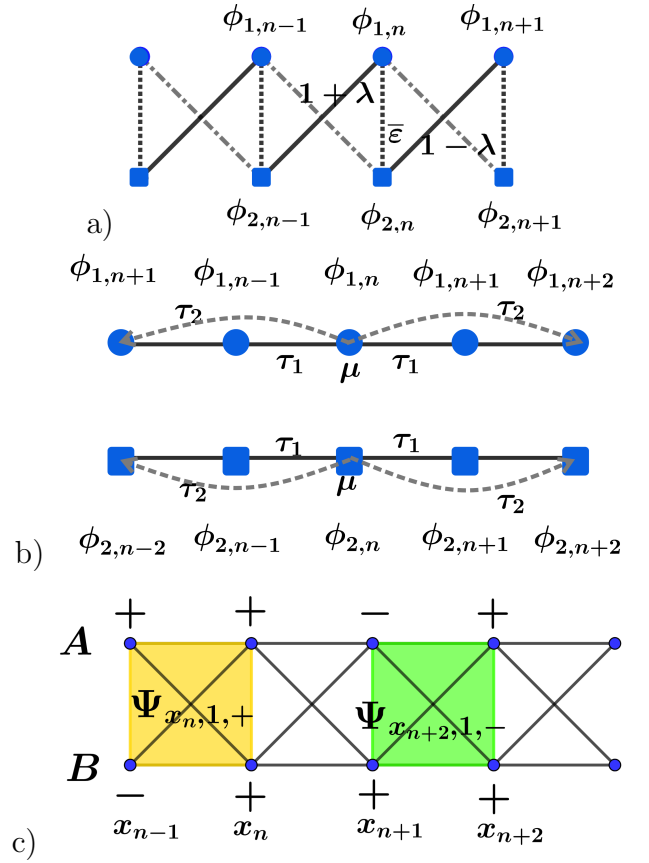


FIG. 4. a) Effective ladder obtained with the change of basis (Eq. (21)) from the original Kitaev-Creutz type ladder. Pictorially, we showed that this effective ladder is composed of two interacting SSH chains. b) Under the renormalization in Eqs. (22, 23), the effective ladder is decomposed into two chains with first- and second-neighbor interaction. In the limit, $\lambda \rightarrow \pm 1$ and $\bar{\varepsilon} = 0$, we obtain the CLS in each site. c) Filled regions show the two CLS in the flat band regime for the valence and conduction regime, and the signs indicate the signs of the CSL amplitudes of their components.

Sites on one sublattice, say A , have the diagonal hopping t_{AA} to the left and t_{BA} to their right, and for sites belonging to the B sublattice, it is just the opposite. From the assumptions in Eq. (4), the time-independent Schrödinger equation can be cast in the equivalent difference equation forms for any pair of sites $(A, n), (B, n)$ as the following pairs of equations:

$$\begin{aligned} (E - \varepsilon)\psi_{A,n} &= t_{AA} (\psi_{A,n-1} + \psi_{A,n+1}) \\ &\quad + t_{AB} (\psi_{B,n+1} - \psi_{B,n-1}) \\ (E + \varepsilon)\psi_{B,n} &= -t_{AA} (\psi_{B,n+1} + \psi_{B,n-1}) \\ &\quad + t_{AB} (\psi_{A,n-1} - \psi_{A,n+1}) \end{aligned} \quad (19)$$

We change the basis defining $\phi_{1,n} = \psi_{A,n} + \psi_{B,n}$ and $\phi_{2,n} = \psi_{A,n} - \psi_{B,n}$. Then, from Eq. (19) we arrive at a

simpler set of equations in this new basis, viz.

$$\begin{aligned} E\phi_{1,n} - \varepsilon\phi_{2,n} &= (t_{AA} - t_{AB})\phi_{2,n+1} + (t_{AA} + t_{AB})\phi_{2,n-1} \\ E\phi_{2,n} - \varepsilon\phi_{1,n} &= (t_{AA} + t_{AB})\phi_{1,n+1} + (t_{AA} - t_{AB})\phi_{1,n-1} \end{aligned} \quad (20)$$

or, equivalently

$$\begin{aligned} \bar{E}\phi_{1,n} - \bar{\varepsilon}\phi_{2,n} &= (1 - \lambda)\phi_{2,n+1} + (1 + \lambda)\phi_{2,n-1} \\ \bar{E}\phi_{2,n} - \bar{\varepsilon}\phi_{1,n} &= (1 + \lambda)\phi_{1,n+1} + (1 - \lambda)\phi_{1,n-1} \end{aligned} \quad (21)$$

where $\bar{E} = E/t_{AA}$. Using the second equation in the first, and vice-versa, the Eq. (20) can be rewritten as

$$\begin{aligned} (\bar{E} - \mu)\phi_{j,n} &= \tau_1(\phi_{j,n-1} + \phi_{j,n+1}) \\ &+ \tau_2(\phi_{j,n+2} + \phi_{j,n-2}), \quad j = 1, 2. \end{aligned} \quad (22)$$

with

$$\begin{aligned} \mu &= \frac{\bar{\varepsilon}^2 + 2(1 + \lambda^2)}{\bar{E}} \\ \tau_1 &= \frac{2\bar{\varepsilon}}{\bar{E}} \\ \tau_2 &= \frac{1 - \lambda^2}{\bar{E}}. \end{aligned} \quad (23)$$

The dispersion relations obtained from the Eq. (22) are easily obtained. The result is the same that in Eq. (15)

$$\begin{aligned} \bar{E} &= \mu + 2\tau_1 \cos(kl) + 2\tau_2 \cos(2kl) \\ \bar{E}_{\pm} &= \pm \sqrt{(\bar{\varepsilon} + 2\cos(kl))^2 + 4\lambda^2 \sin^2(kl)} \end{aligned} \quad (24)$$

A look at the Eq. (22) shows that the change of basis from $\psi_n \rightarrow \phi_n$ casts the pair of original equations in Eq. (19) into a pair of equations, each representing a single, perfectly periodic chain with hopping to first-, τ_1 , and second- neighbors, τ_2 ; and an effective on-site energy μ .

The set of Eqs. (23) immediately reveals that if we select either $(\bar{\varepsilon}, \lambda) = (0, 1)$ or $(\bar{\varepsilon}, \lambda) = (0, -1)$, the right-hand side of Eq. (22) becomes zero and, consequently, Eq. (22) admits a *localized* atomic-like state at energy, which is the solution of the equation $\bar{E} - \mu = 0$, that is, at $\bar{E} = \pm 2$. This is a CLS and gives a flat band.

2. CLS from k -space.

As we shown, the eigenvalues of the Hamiltonian Eq. (6) consist of two flat-bands (FB) $\epsilon(k) = \pm 2$ when $\bar{\varepsilon} = 0$ and $\lambda = \pm 1$. The Bloch state creation operator related to the FB takes the form

$$\Psi_{k,\lambda,\pm}^\dagger = \frac{1}{2} \left\{ (1 \pm e^{-\lambda k}) a_k^\dagger + (1 \mp e^{-\lambda k}) b_k^\dagger \right\} \quad (25)$$

where the sign \pm is for $\epsilon(k) = \pm 2$, respectively.

Firstly, note that because of the energy degeneracy, any linear combination of the FB Bloch states is still an

eigenstate. Particularly, the Fourier transform of the FB Bloch states should be eigenstates. For example, let us calculate the Fourier transform of Eq. (25)

$$\begin{aligned} \Psi_{\mathbf{x}_n,\lambda,\pm} &= \mathcal{N} \int_{BZ} dk e^{ik\mathbf{x}_n} \Psi_{k,\lambda,\pm}^\dagger \\ &= \frac{1}{2} \left(a_n^\dagger \pm a_{n-\lambda}^\dagger + b_n^\dagger \mp b_{n-\lambda}^\dagger \right) \end{aligned} \quad (26)$$

where \mathcal{N} is a normalization constant. As shown in Fig. $\Psi_{\mathbf{x}_n,\lambda,\pm}$ takes the form of a localized square plaquette. One can verify that the sites of plaquettes obey the following relations, analogous to Landau Levels states relations in a magnetic lattice with one flux quantum per unit cell [27],

$$\begin{aligned} \sum_{\mathbf{x}_n} (-1)^n \Psi_{\mathbf{x}_n,\lambda,+}^{(1)} + \Psi_{\mathbf{x}_n,\lambda,+}^{(2)} &= 0 \\ \sum_{\mathbf{x}_n} \Psi_{\mathbf{x}_n,\lambda,-}^{(1)} + (-1)^n \Psi_{\mathbf{x}_n,\lambda,-}^{(2)} &= 0 \end{aligned} \quad (27)$$

with $\Psi^{(1,2)}$ as the first- and second- component of the FB Bloch state. Consequently, this kind of destructive interference effectively traps the electron within the plaquette. The electron thus appears to have a quenched kinetic energy as dictated by FB.

C. Topological properties I: winding number

The Hamiltonian (6) is highly symmetric. It anti-commutes with the ‘particle-hole’ symmetry $\mathcal{P} = \sigma_x \mathcal{K}$, where \mathcal{K} accounts for complex conjugation. The time reversal for spinless fermions is also present and is given by $\mathcal{T} = \mathbb{1}\mathcal{K}$.

Finally, the product of $\mathcal{T}\mathcal{P} = \mathcal{C} = \sigma_x$ is the chiral symmetry, whose presence allows us to define the topological invariant in terms of the winding number [45]. Note that all symmetries place the chain model in the BDI class [46].

The winding number is given by [45, 46]

$$\nu = \frac{1}{2\pi} \int_{-\pi/l}^{\pi/l} dk \partial_k \omega_k, \quad (28)$$

here $\partial_k \omega_k$ is the winding number density. A trivial phase corresponds to $\nu = 0$, a non-trivial one to finite integer values of ν . The winding number relates the bulk properties to the existence of boundary states in a finite chain. This property is known as bulk-edge correspondence. Due to their topological nature, their existence is robust against small perturbations, like disorder. The phase diagram constructed using the winding number invariant is shown in Fig. 5.

The boundaries between different topological phases can be obtained from the condition of closing the bulk gap, i.e., $\epsilon(k) = 0$ (cf Eq. (16)). That is only possible if both terms under the square root vanish. The condition

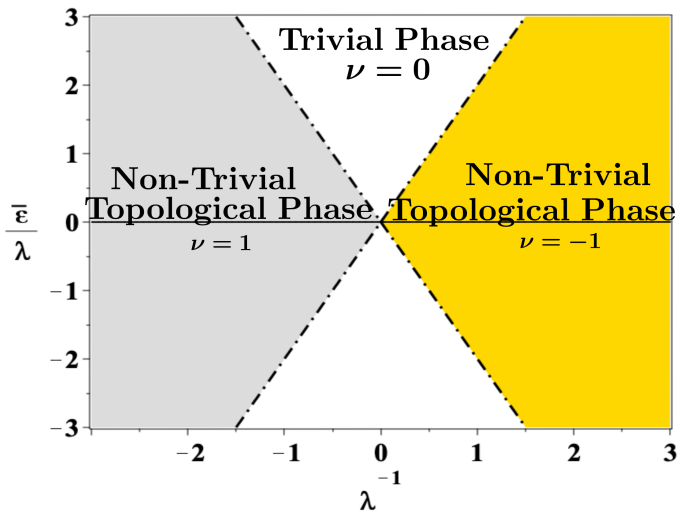


FIG. 5. Topological phase diagram of the Kitaev-Creutz type ladder, constructed with the winding number invariant equation (28). Distinct topological phases are separated by the phase boundary at $\bar{\epsilon} = \pm 2$, visualized by the dashed black lines.

of $\lambda \neq 0$ forces the gap closing to occur at $kl = 0, \pm\pi d$, and the remaining term vanishes at these momenta if $\bar{\epsilon} = \pm 2$.

In addition, we show in Fig. 6 the geometrical representation of the function $\mathbf{n}(\mathbf{k})$ (cf. Eq. (8)) along the Brillouin Zone (BZ) projected to the $(n_y(k), n_z(k))$ plane for simplicity, and thus the topological corresponds to its winding number around the origin with different values of $\bar{\epsilon}$ and λ .

D. Topological properties II: *Fubini-Study* metric.

Let us start by considering a quantum state $|\psi(\boldsymbol{\xi})\rangle$, which depends on a set of parameters $\boldsymbol{\xi} = (\xi_1, \xi_2, \dots, \xi_N)$, where N is the dimension of the parameter space. The quantum metric (or *FS* metric) $g_{\mu\nu}(\boldsymbol{\xi})$ defined in this parameter space originates from the so-called quantum geometric tensor [47–52]

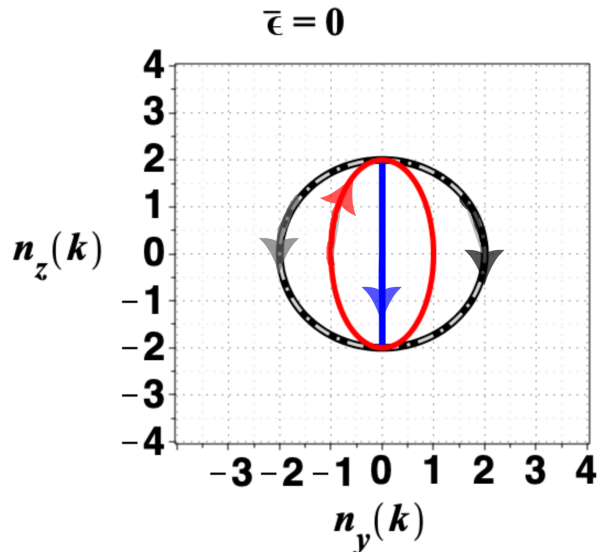
$$Q_{\mu\nu}(\boldsymbol{\xi}) \equiv \langle \partial_\mu \psi(\boldsymbol{\xi}) | \mathbb{P}_{\psi(\boldsymbol{\xi})} | \partial_\nu \psi(\boldsymbol{\xi}) \rangle \quad (29)$$

which defines a gauge-invariant quantity associated with $|\psi(\boldsymbol{\xi})\rangle$ and $\mathbb{P}_{\psi(\boldsymbol{\xi})}$ is the orthogonal complement projector, given by

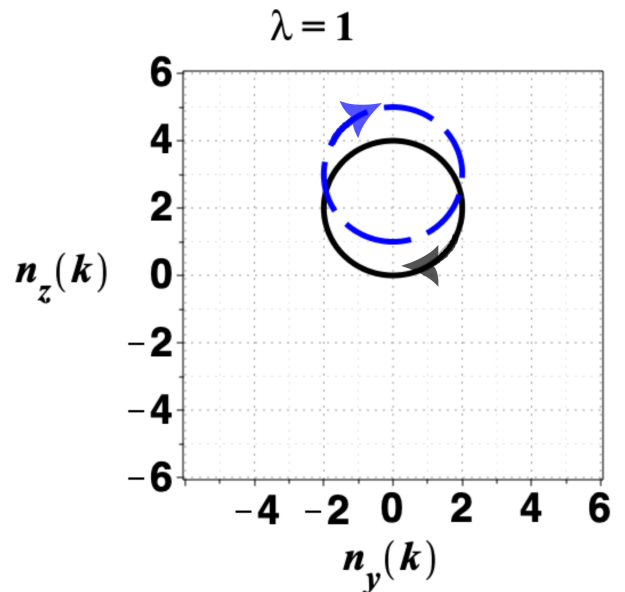
$$\mathbb{P}_{\psi(\boldsymbol{\xi})} = \mathbb{1} - |\psi(\boldsymbol{\xi})\rangle \langle \psi(\boldsymbol{\xi})|. \quad (30)$$

The tensor $Q_{\mu\nu}$ can take complex values: The real part defines the quantum metric $g_{\mu\nu}(\boldsymbol{\xi}) = \text{Re}[Q_{\mu\nu}(\boldsymbol{\xi})]$, while the imaginary part is related to the Berry curvature $\Omega_{\mu\nu}(\boldsymbol{\xi})$ with

$$\text{Im}[Q_{\mu\nu}] = -\frac{\Omega_{\mu\nu}}{2}. \quad (31)$$



a)



b)

FIG. 6. a) Image of the function $(n_y(k), n_z(k))$ (cf Eq. (8)) along the Brillouin zone for some of the points in the phase diagram (see Fig. 5). Its winding number around the origin corresponds to the topological invariant ν . a) For this figure we set $\bar{\epsilon} = 0$ and $\lambda = -1$ (gray circle), $\lambda = 0$ (blue line), $\lambda = 1/2$ (red ellipse), $\lambda = 1$ (black circle); and for b) we choose $\lambda = 1$ and $\bar{\epsilon} = 2$ (black circle) and $\bar{\epsilon} = 3$ (blue dashed circle). We note that for the blue line in a) and the black circle in b), ν is not well defined because the image of the function passes through the origin.

The *FS* metric provides a distance between nearby states $|\psi(\boldsymbol{\xi})\rangle$ and $|\psi(\boldsymbol{\xi} + d\boldsymbol{\xi})\rangle$, i.e. the distinguishability of pure quantum states in the sense of a statistical distance [53].

Now, if we choose the Bloch states given by

$$\begin{aligned} |u_k^+\rangle &= (\cos(\omega_k/2), i \sin(\omega_k/2))^T, \text{ for conduction band} \\ |u_k^-\rangle &= (i \sin(\omega_k/2), \cos(\omega_k/2))^T, \text{ for valence band,} \end{aligned} \quad (32)$$

then, the derivatives are

$$\begin{aligned} |\partial_k u_k^+\rangle &= \frac{\partial_k \omega_k}{2} (-\sin(\omega_k/2), i \cos(\omega_k/2))^T, \\ |\partial_k u_k^-\rangle &= \frac{\partial_k \omega_k}{2} (i \cos(\omega_k/2), -\sin(\omega_k/2))^T. \end{aligned} \quad (33)$$

and following the formula for the FS metric, it can be proved that [53, 54]

$$\begin{aligned} g_{kk}^\pm &= \langle \partial_k u_k^\pm | \partial_k u_k^\pm \rangle - \langle \partial_k u_k^\pm | u_k^\pm \rangle \langle u_k^\pm | \partial_k u_k^\pm \rangle \\ &= \left(\frac{\partial_k \omega_k}{2} \right)^2. \end{aligned} \quad (34)$$

The first observation is that from Eq. (34) it follows

$$\sqrt{\det(g_{kk}^\pm)} = \frac{|\partial_k \omega_k|}{2}. \quad (35)$$

We define the quantities $\text{vol}(\text{BZ})$ and $\text{vol}(S^1)$ given by

$$\begin{aligned} \text{vol}(\text{BZ}) &\equiv \int_{\text{BZ}} \sqrt{\det(g_{kk}^\pm)} dk \\ \text{Vol}(S^1) &\equiv \int_{S^1} d\theta. \end{aligned} \quad (36)$$

In the case where the FS metric are nondegenerate, $\text{vol}(\text{BZ})$ and $\text{vol}(S^1)$ correspond to the *volumes* of the Brillouin Zone (BZ) and the unitary circle S^1 , respectively. Thus, we obtained from Eqs. (28, 35, 36) the following inequalities

$$\pi|\nu| \leq \text{vol}(\text{BZ}) \leq \frac{1}{2} \text{vol}(S^1). \quad (37)$$

In other words, the winding number of the occupied Bloch bundle determines the minimal quantum volume. It is equivalent to that found by Ozawa and Mera in the 2D case, where the equalities are associated with a flat Kähler structure [34–36]. Furthermore, the 2D version has been applied to topological superconductors to find a relation between the superfluid weight and the topological properties of the system [55–60].

On the hand, in order to understand the geometry related to the FS metric tensor, g_{kk}^\pm , it is necessary to consider the FS arc element ds_{FS} and the usual infinitesimal line elements on S^1 , ds_{S^1} , which are given by

$$\begin{aligned} ds_{FS}^2 &= g_{kk}^\pm dk^2 = \left(\frac{1}{2} \right)^2 d\omega_k^2, \quad |k| \leq \pi/l \\ ds_{S^1}^2 &= d\theta^2, \quad |\theta| \leq \pi \end{aligned} \quad (38)$$

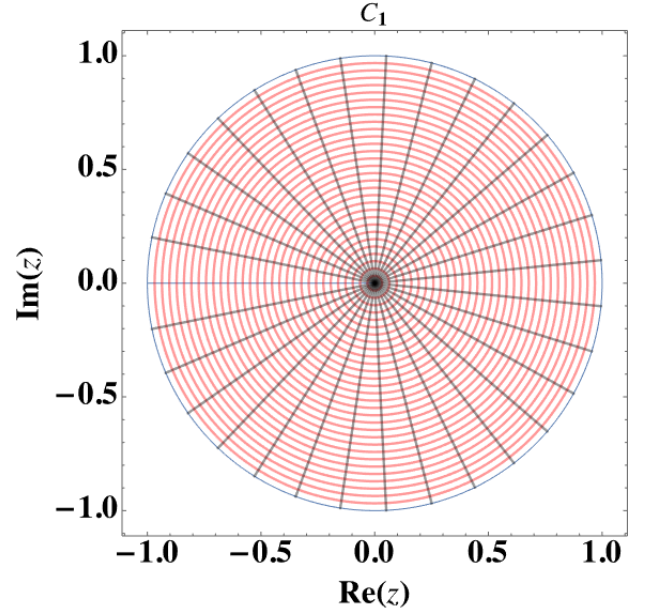


FIG. 7. Complex plane \mathbb{C}_1 under the relation \triangleright (Eq. (39)), which can be interpreted as each state z on a specific external ray are element of the one equivalence class, $[z]$. Thus, there exists an isomorphism between \mathbb{C}_1 and S^1 (blue circle) and the distance between two equivalence class $[z_1]$ and $[z_2]$ is given by the angular difference between the respective external rays (cf. Eq. (38)). In this space, the distance between any two adjacent external rays shown in the figure is the same.

Thus, from Eq. 38, we show that there is a locally conformal transformation between S^1 to the FS manifold. Furthermore, we can conceive the space FS and S^1 as embeddings in the complex plane with an additional structure given by the equivalence relation \triangleright on \mathbb{C} ,

$$z_1 \triangleright z_2 \text{ if } |z_1| = |R||z_2| \text{ and } \text{Arg}(z_1) = \text{Arg}(z_2) \quad (39)$$

where $|R|$ is a scale factor; i.e., z_1 and z_2 are on the same external ray. In addition, let us consider the mapping f defined by

$$\begin{aligned} f : \mathbb{C}_1 &\rightarrow \mathbb{C}_2 \\ z = r e^{ik} &\mapsto w = f(z) = \frac{r}{2} e^{i\omega_k} \end{aligned} \quad (40)$$

where the indexes refer to the first and second copies of the complex plane, respectively. Therefore, if we consider the usual infinitesimal line element on \mathbb{C}

$$ds_{\mathbb{C}}^2 = dz dz^* = dr^2 + r^2 d\theta^2, \quad z = r e^{i\theta} \quad (41)$$

where $*$ is the complex conjugate, we obtain that \mathbb{C}_1 and \mathbb{C}_2 under the relation \triangleright , are isomorphic to S^1 (see Fig. 7) and FS manifold (see Figs. 8, 9), respectively.

Then, in Figs. 8 and 9 a)-c), we show the maps \mathbb{C}_1 onto \mathbb{C}_2 under f given by Eq. (40) with different values $\bar{\varepsilon}$ and λ ; a first observation is that f preserves circles and external rays only in the nontrivial topological regime,

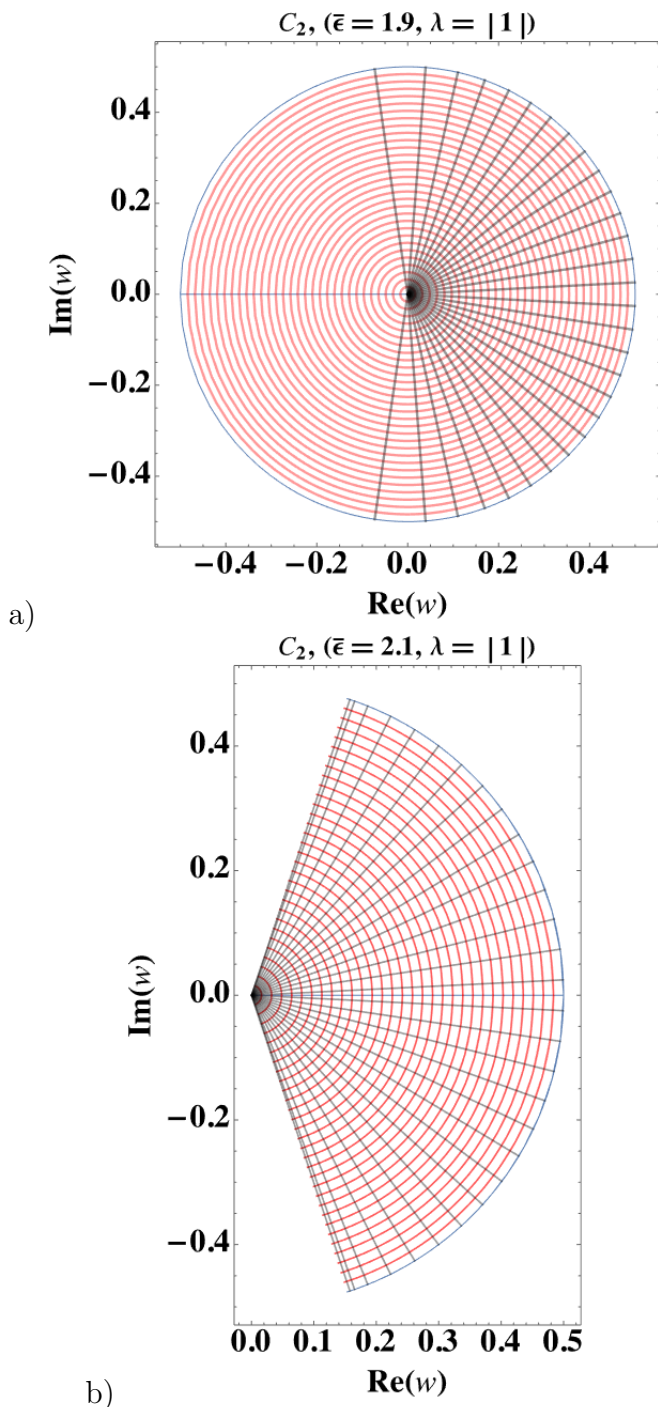


FIG. 8. Image of \mathbb{C}_1 (Fig. 7) under the mapping f (Eq. (40)) with the values $\lambda = |1|$ and a) $\bar{\varepsilon} = 1.9$, b) $\bar{\varepsilon} = 2.1$. It can be observed that, in the non-trivial topological regime, $|\bar{\varepsilon}| \leq 2$, f maps rays and circles from \mathbb{C}_1 (see Fig. 7) to rays and circles with half the radius, respectively. Meanwhile, in the trivial topological regime, circles are deformed to be mapped onto arcs of circles, given another geometrical perspective of Eq. (28). The inequality in Eq. (37) manifests a clear geometrical interpretation in these figures. Thus, $\text{vol}(BZ)$ (cf. Eq. (36)) corresponds to the perimeter of the blue circle (or arc circle), respectively; therefore, in the topological regime the equality holds (a), contrary to the non-topological regime (b)) in which the strict inequality hold.

but deforms circles onto arcs of circles, given another geometrical perspective of Eq. (28). This mapping also allows for a visual realization of inequality Eq. (37), in which $\text{vol}(BZ)$ corresponds exactly to the perimeter of the blue circle (or arc circle), respectively (see Fig. 8).

However, as we show in Fig. 9 a)-c), f does deform the distribution of rays, which is related to the FS metric tensor, g_{kk}^{\pm} . For example, in the case of Fig. 9 b) where $\lambda = 0.5$, the external rays appear to separate near the angles $k = \pm\pi/2$ and correspond to the maxima of g_{kk}^{\pm} as shown in Fig. 9 d). In a similar form, in the case of Fig. 9 c) where $\lambda = |3|$ for $k = 0, \pm\pi$. Something noteworthy about this geometric representation is that although all 3 systems have a nontrivial topology with $|\nu| = 1$, the FS metric allows us to establish differences between them. In particular, system Fig. 9 a) corresponding to the regime of flat bands is the only system in which the distribution of rays is not deformed under f .

This can be confirmed as in the FB regime the FS metric is constant as,

$$\partial_k \omega_k(\lambda = \pm 1) = \pm l \quad (\text{cf. (A7)}) \quad (42)$$

and thus is equivalent to the usual metric over S^1 . Such equivalence is readily found from the fact that an arc element ds of a geodesic in the FS manifold is given by,

$$ds^2 = \left(\frac{l}{2}\right)^2 dk^2 \quad (43)$$

equivalent to an arc element of a circle with a radius $l/2$.

IV. CONCLUSIONS.

In conclusion, we have shown a mapping between a chain with $s - p$ orbitals onto a Kitaev-Creutz type model. With this map, we have found the existence of Bogoliubov-like modes and compact localized states in the flat band (FB) regime which obeys an analogous Landau relation (cf. Eq. (27)). In addition, we obtained that there is a non-trivial topological transition by the condition $\bar{\varepsilon} = \pm 2$ (see Fig. 5) that results in a non-trivial winding number. Furthermore, our analysis reveals the fingerprint of the flat bands with the FS metric that allows us to distinguish between pure states of systems with the same topology, in particular, in this model the FS metric is equivalent to the usual metric over S^1 in the FB regime.

These results could have potential implications for the development of simpler models that contribute to a better understanding of the formation of flat bands and their implications in the many-body interaction regime.

ACKNOWLEDGMENT.

A.E.C. thanks to the CONACyT scholarship for providing financial support. This work was supported

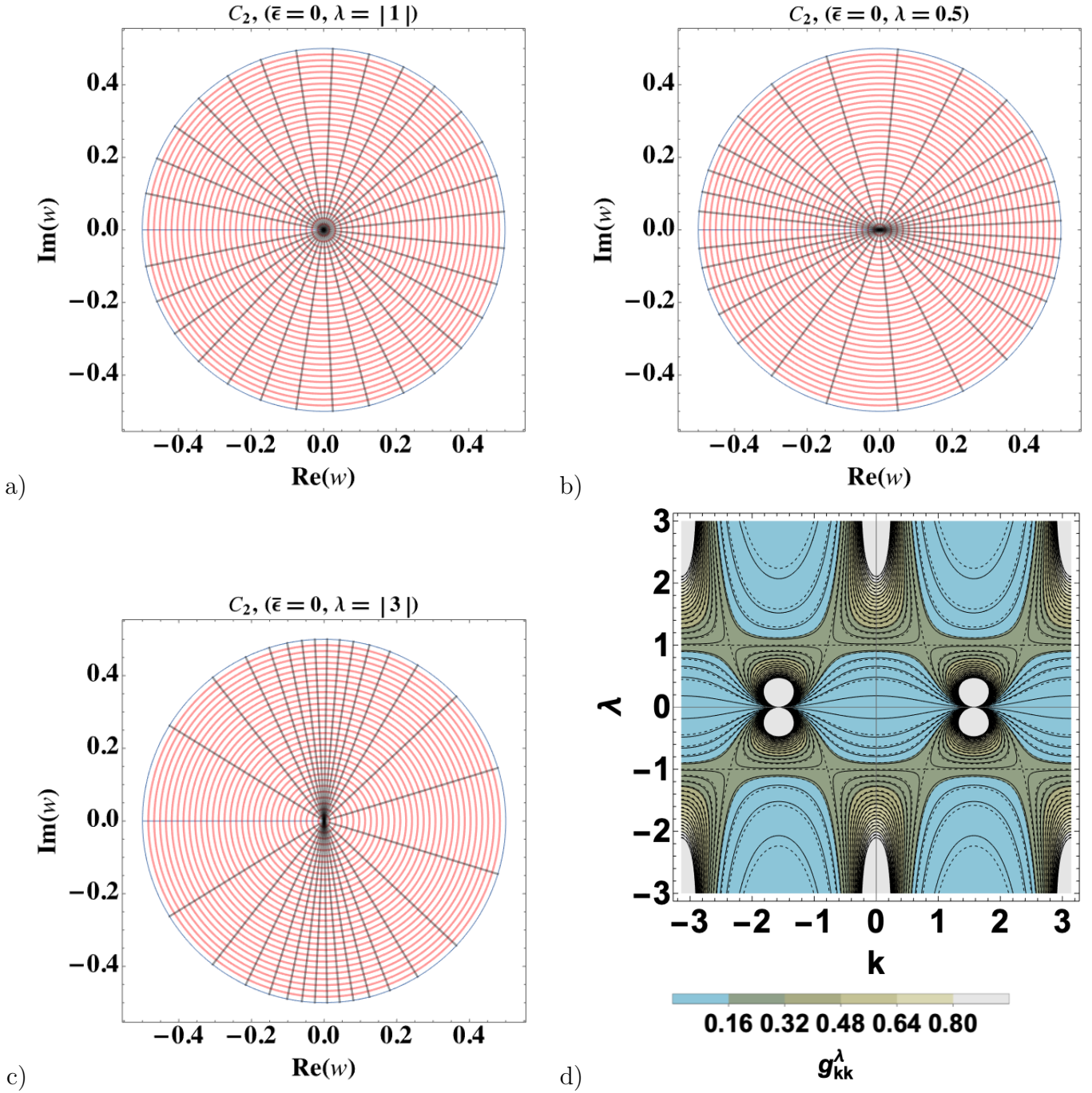


FIG. 9. Image of \mathbb{C}_1 (Fig. 7) under the mapping f (Eq. (40)) with the values $\bar{\epsilon} = 0$ and a) $\lambda = |1|$, b) $\lambda = 0.5$ and c) $\lambda = |3|$, while in d) it is shown a contour plot of the metric tensor g_{kk}^\pm given by Eq. (34) as a function of λ and k with $\bar{\epsilon} = 0$. As discussed, the mapping f preserves circles and external rays in the topological regime (see Fig. 8); however, as can be observed in images a)-c), f does deform the distribution of rays, which is related to the FS metric tensor, g_{kk}^\pm . For example, in the case of c) where $\lambda = |3|$, the external rays appear to separate near the angles $k = 0, \pm\pi$ and correspond to the maxima of g_{kk}^\pm as shown in d). Something noteworthy about this geometric representation is that although all 3 systems have a nontrivial topology with $|\nu| = 1$, the FS metric allows us to establish differences between them. In particular, system a) corresponding to the regime of flat bands is the only system in which the distribution of rays is not deformed under f .

by UNAM DGAPA PAPIIT IN102620 and CONACyT project 1564464.

Appendix A: Bogoulibov transformation.

We define a Bogoulibov-like modes γ_k, ϱ_k as

$$\begin{aligned}\gamma_k &\equiv u_k a_k + v_k b_k \\ \varrho_k &\equiv -v_k^* a_k + u_k^* b_k\end{aligned}\quad (\text{A1})$$

and the anti-commutation relations for γ_k are

$$\begin{aligned}\{\gamma_k, \gamma_{k'}^\dagger\} &= (u_k a_k + v_k b_k) (u_{k'}^* a_{k'}^\dagger + v_{k'}^* b_{k'}^\dagger) \\ &+ (u_{k'}^* a_{k'}^\dagger + v_{k'}^* b_{k'}^\dagger) (u_k a_k + v_k b_k) \\ &= u_k u_{k'}^* \{a_k, a_{k'}^\dagger\} + v_k v_{k'}^* \{b_k, b_{k'}^\dagger\} \\ &+ u_k v_{k'}^* \{a_k, b_{k'}^\dagger\} + u_{k'}^* v_k \{b_k, a_{k'}^\dagger\} \\ &= (u_k u_{k'}^* + v_k v_{k'}^*) \delta_{kk'} \\ &= \delta_{kk'}, \text{ if } |u_k|^2 + |v_k|^2 = 1\end{aligned}\quad (\text{A2})$$

$$\begin{aligned}\{\gamma_k, \gamma_{k'}\} &= (u_k a_k + v_k b_k) (u_{k'} a_{k'} + v_{k'} b_{k'}) \\ &+ (u_{k'} a_{k'} + v_{k'} b_{k'}) (u_k a_k + v_k b_k) \\ &= u_k u_{k'} \{a_k, a_{k'}\} + v_k v_{k'} \{b_k, b_{k'}\} \\ &+ u_k v_{k'} \{a_k, b_{k'}\} + u_{k'} v_k \{b_k, a_{k'}\} \\ &= 0\end{aligned}\quad (\text{A3})$$

$$\begin{aligned}\{\gamma_k^\dagger, \gamma_{k'}^\dagger\} &= (u_k^* a_k^\dagger + v_k^* b_k^\dagger) (u_{k'}^* a_{k'}^\dagger + v_{k'}^* b_{k'}^\dagger) \\ &+ (u_{k'}^* a_{k'}^\dagger + v_{k'}^* b_{k'}^\dagger) (u_k^* a_k^\dagger + v_k^* b_k^\dagger) \\ &= u_k^* u_{k'}^* \{a_k^\dagger, a_{k'}^\dagger\} + v_k^* v_{k'}^* \{b_k^\dagger, b_{k'}^\dagger\} \\ &+ u_k^* v_{k'}^* \{a_k^\dagger, b_{k'}^\dagger\} + u_{k'}^* v_k^* \{b_k^\dagger, a_{k'}^\dagger\} \\ &= 0\end{aligned}\quad (\text{A4})$$

and similar anticommutation relations for ϱ_k under the interchange of $u_k \leftrightarrow -v_k^*$ and $v_k \leftrightarrow u_k^*$. From the definition, (A1) we can obtain the following result

$$\begin{aligned}\epsilon(k) (\gamma_k^\dagger \gamma_k - \varrho_k^\dagger \varrho_k) &= \epsilon(k) \left[(u_k^* a_k^\dagger + v_k^* b_k^\dagger) (u_k a_k + v_k b_k) \right. \\ &\quad \left. - (-v_k a_k^\dagger + u_k b_k^\dagger) (-v_k^* a_k + u_k^* b_k) \right] \\ &= \epsilon(k) \left[(|u_k|^2 - |v_k|^2) a_k^\dagger a_k + \right. \\ &\quad \left. - (|u_k|^2 - |v_k|^2) b_k^\dagger b_k + 2u_k^* v_k a_k^\dagger b_k \right. \\ &\quad \left. + 2u_k v_k^* b_k^\dagger a_k \right]\end{aligned}\quad (\text{A5})$$

If we choose u_k and v_k as

$$\begin{aligned}u_k &\equiv \cos\left(\frac{\omega_k}{2}\right), \\ v_k &\equiv -i \sin\left(\frac{\omega_k}{2}\right), \\ \sin(\omega_k) &\equiv \frac{2\lambda \sin(kl)}{\epsilon(k)}, \\ \cos(\omega_k) &\equiv \frac{\bar{\epsilon} + 2 \cos(kl)}{\epsilon(k)}, \\ \epsilon(k) &= \sqrt{(\bar{\epsilon} + 2 \cos(kl))^2 + (2\lambda \sin(kl))^2}.\end{aligned}\quad (\text{A6})$$

We recover the Hamiltonian form of Eq. (6). We note that only the two cases $\bar{\epsilon} = 0, \lambda = \pm 1$, the relation ω_k with k is linear, i.e.

$$\omega_k = \pm kl, \text{ if } \lambda = \pm 1 \text{ and } \bar{\epsilon} = 0. \quad (\text{A7})$$

-
- [1] Daniel Leykam, Alexei Andreanov, and Sergej Flach. Artificial flat band systems: from lattice models to experiments. *Advances in Physics: X*, 3(1):1473052, Jan 2018.
- [2] Wen-Xuan Qiu, Shuai Li, Jin-Hua Gao, Yi Zhou, and Fu-Chun Zhang. Designing an artificial lieb lattice on a metal surface. *Phys. Rev. B*, 94:241409, Dec 2016.
- [3] Robert Drost, Teemu Ojanen, Ari Harju, and Peter Liljeroth. Topological states in engineered atomic lattices. *Nature Physics*, 13(7):668–671, Jul 2017.
- [4] C. C. Abilio, P. Butaud, Th. Fournier, B. Pannetier, J. Vidal, S. Tedesco, and B. Dalzotto. Magnetic field induced localization in a two-dimensional superconducting wire network. *Phys. Rev. Lett.*, 83:5102–5105, Dec 1999.
- [5] Shintaro Taie, Hideki Ozawa, Tomohiro Ichinose, Takuei Nishio, Shuta Nakajima, and Yoshiro Takahashi. Coherent driving and freezing of bosonic matter wave in an optical lieb lattice. *Science Advances*, 1(10):e1500854, 2015.
- [6] Yosuke Nakata, Takanori Okada, Toshihiro Nakanishi, and Masao Kitano. Observation of flat band for terahertz spoof plasmons in a metallic kagomé lattice. *Phys. Rev. B*, 85:205128, May 2012.
- [7] Yanyan He, Ruosong Mao, Han Cai, Jun-Xiang Zhang, Yongqiang Li, Luqi Yuan, Shi-Yao Zhu, and Da-Wei Wang. Flat-band localization in creutz superradiance lattices. *Physical Review Letters*, 126(10):103601, Mar 2021.
- [8] Gerardo G. Naumis, Leonardo A. Navarro-Labastida, Enrique Aguilar-Méndez, and Abdiel Espinosa-Champo. Reduction of the twisted bilayer graphene chiral hamiltonian into a 2×2 matrix operator and physical origin of flat bands at magic angles. *Phys. Rev. B*, 103:245418, Jun 2021.
- [9] Leonardo A. Navarro-Labastida, Abdiel Espinosa-Champo, Enrique Aguilar-Mendez, and Gerardo G. Naumis. Why the first magic-angle is different from others in twisted graphene bilayers: Interlayer currents, kinetic and confinement energy, and wave-function localization. *Phys. Rev. B*, 105:115434, Mar 2022.
- [10] Andreas Mielke and Hal Tasaki. Ferromagnetism in the hubbard model. *Communications in Mathematical Physics*, 158(2):341–371, Nov 1993.
- [11] Hal Tasaki. From nagaoka’s ferromagnetism to flat-band ferromagnetism and beyond: An introduction to ferromagnetism in the hubbard model. *Progress of Theoretical Physics*, 99(4):489–548, Apr 1998.
- [12] Yuan Cao, Valla Fatemi, Shiang Fang, Kenji Watanabe, Takashi Taniguchi, Efthimios Kaxiras, and Pablo Jarillo-Herrero. Unconventional superconductivity in magic-angle graphene superlattices. *Nature*, 556(7699):43–50, 2018.
- [13] Hideo Aoki. Theoretical possibilities for flat band superconductivity. *Journal of Superconductivity and Novel Magnetism*, 33(8):2341–2346, 2020.
- [14] Congjun Wu, Doron Bergman, Leon Balents, and S. Das Sarma. Flat bands and wigner crystallization in the honeycomb optical lattice. *Phys. Rev. Lett.*, 99:070401, Aug 2007.
- [15] Błażej Jaworowski, Alev Devrim Güçlü, Piotr Kaczmarkiewicz, Michał Kupczyński, Paweł Potasz, and Arkadiusz Wójs. Wigner crystallization in topological flat bands. *New Journal of Physics*, 20(6):063023, jun 2018.
- [16] M.D. Settle, R.J.P. Engelen, M. Salib, A. Michaeli, L. Kuipers, and T.F. Krauss. Flatband slow light in photonic crystals featuring spatial pulse compression and terahertz bandwidth. *Opt. Express*, 15(1):219–226, Jan 2007.
- [17] T F Krauss. Slow light in photonic crystal waveguides. *Journal of Physics D: Applied Physics*, 40(9):2666, apr 2007.
- [18] Emil J. Bergholtz and Zhao Liu. Topological flat band models and fractional chern insulators. *International Journal of Modern Physics B*, 27(24):1330017, Sep 2013.
- [19] H. S. Nguyen, F. Dubois, T. Deschamps, S. Cueff, A. Pardon, J.-L. Leclercq, C. Seassal, X. Letartre, and P. Viktorovitch. Symmetry breaking in photonic crystals: On-demand dispersion from flatband to dirac cones. *Phys. Rev. Lett.*, 120:066102, Feb 2018.
- [20] Shuiquan Deng, Arndt Simon, and Jürgen Köhler. The origin of a flat band. *Journal of Solid State Chemistry*, 176(2):412–416, 2003. Special issue on The Impact of Theoretical Methods on Solid-State Chemistry.
- [21] Bill Sutherland. Localization of electronic wave functions due to local topology. *Phys. Rev. B*, 34:5208–5211, Oct 1986.
- [22] Elliott H. Lieb. Two theorems on the hubbard model. *Phys. Rev. Lett.*, 62:1201–1204, Mar 1989.
- [23] A Mielke. Ferromagnetic ground states for the hubbard model on line graphs. *Journal of Physics A: Mathematical and General*, 24(2):L73, jan 1991.
- [24] Hal Tasaki. Ferromagnetism in the hubbard models with degenerate single-electron ground states. *Phys. Rev. Lett.*, 69:1608–1611, Sep 1992.
- [25] Nobuyuki Shima and Hideo Aoki. Electronic structure of super-honeycomb systems: A peculiar realization of semimetal/semiconductor classes and ferromagnetism. *Phys. Rev. Lett.*, 71:4389–4392, Dec 1993.
- [26] Hideo Aoki, Masato Ando, and Hajime Matsumura. Hofstadter butterflies for flat bands. *Phys. Rev. B*, 54:R17296–R17299, Dec 1996.
- [27] Liu Zheng, Liu Feng, and Wu Yong-Zhi. Exotic electronic states in the world of flat bands: From theory to material. *Chinese Physics B*, 23(7):077308, may 2014.
- [28] D. J. Thouless, M. Kohmoto, M. P. Nightingale, and M. den Nijs. Quantized hall conductance in a two-dimensional periodic potential. *Phys. Rev. Lett.*, 49:405–408, Aug 1982.
- [29] N. Regnault and B. Andrei Bernevig. Fractional chern insulator. *Phys. Rev. X*, 1:021014, Dec 2011.
- [30] Siddharth A. Parameswaran, Rahul Roy, and Shivaji L. Sondhi. Fractional quantum hall physics in topological flat bands. *Comptes Rendus Physique*, 14(9):816–839, 2013. Topological insulators / Isolants topologiques.
- [31] Zhi Li, Jincheng Zhuang, Li Wang, Haifeng Feng, Qian Gao, Xun Xu, Weichang Hao, Xiaolin Wang, Chao Zhang, Kehui Wu, Shi Xue Dou, Lan Chen, Zhenpeng Hu, and Yi Du. Realization of flat band with possible nontrivial topology in electronic kagome lattice. *Science Advances*, 4(11):eaau4511, 2018.
- [32] R. B. Laughlin. Anomalous quantum hall effect: An in-

- compressible quantum fluid with fractionally charged excitations. *Phys. Rev. Lett.*, 50:1395–1398, May 1983.
- [33] Patrick J. Ledwith, Eslam Khalaf, and Ashvin Vishwanath. Strong coupling theory of magic-angle graphene: A pedagogical introduction. *Annals of Physics*, 435:168646, 2021. Special issue on Philip W. Anderson.
- [34] Bruno Mera and Tomoki Ozawa. Engineering geometrically flat chern bands with fubini-study kähler structure. *Phys. Rev. B*, 104:115160, Sep 2021.
- [35] Bruno Mera and Tomoki Ozawa. Kähler geometry and chern insulators: Relations between topology and the quantum metric. *Phys. Rev. B*, 104:045104, Jul 2021.
- [36] Tomoki Ozawa and Bruno Mera. Relations between topology and the quantum metric for chern insulators. *Phys. Rev. B*, 104:045103, Jul 2021.
- [37] Sonai Seenithurai and Jeng-Da Chai. Electronic and hydrogen storage properties of li-terminated linear boron chains studied by tao-dft. *Scientific Reports*, 8(1):13538, 2018.
- [38] Vidya Kochat, Atanu Samanta, Yuan Zhang, Sanjit Bhowmick, Praveena Manimunda, Syed Asif S. Asif, Anthony S. Stender, Robert Vajtai, Abhishek K. Singh, Chandra S. Tiwary, and Pulickel M. Ajayan. Atomically thin gallium layers from solid-melt exfoliation. *Science Advances*, 4(3):e1701373, 2018.
- [39] Mohd Ishtiyak, Gopabandhu Panigrahi, Subhendu Jana, Jai Prakash, Adel Mesbah, Christos D. Malliakas, Sébastien Lebègue, and James A. Ibers. Modulated linear tellurium chains in ba₃sct₅: Synthesis, crystal structure, optical and resistivity studies, and electronic structure. *Inorganic Chemistry*, 59(4):2434–2442, 02 2020.
- [40] W.A. Harrison. *Electronic Structure and the Properties of Solids: The Physics of the Chemical Bond*. Dover Books on Physics. Dover Publications, 1989.
- [41] Steven M. Girvin and Kun Yang. *Modern Condensed Matter Physics*. Cambridge University Press, 2019.
- [42] K. Thirulogasanthar and B. Muraleetharan. Canonical, squeezed and fermionic coherent states in a right quaternionic hilbert space with a left multiplication on it. In Jean-Pierre Antoine, Fabio Bagarello, and Jean-Pierre Gazeau, editors, *Coherent States and Their Applications*, pages 135–155, Cham, 2018. Springer International Publishing.
- [43] Leonardo A. Navarro-Labastida and Gerardo G. Naumis. The hidden connection between twisted bilayer graphene and the quantum hall effect: Zero flat band electronic modes converge into coherent landau level states and its resultant 3/2 magic-angle quantization rule. *arXiv*, 2022.
- [44] Jun-Won Rhim and Bohm-Jung Yang. Singular flat bands. *Advances in Physics: X*, 6(1):1901606, Jan 2021.
- [45] S. N. Kempkes, M. R. Slot, J. J. van den Broeke, P. Capiod, W. A. Benalcazar, D. Vanmaekelbergh, D. Bercioux, I. Swart, and C. Morais Smith. Robust zero-energy modes in an electronic higher-order topological insulator. *Nature Materials*, 18(12):1292–1297, 2019.
- [46] Ching-Kai Chiu, Jeffrey C. Y. Teo, Andreas P. Schnyder, and Shinsei Ryu. Classification of topological quantum matter with symmetries. *Rev. Mod. Phys.*, 88:035005, Aug 2016.
- [47] Tomoki Ozawa and Nathan Goldman. Extracting the quantum metric tensor through periodic driving. *Phys. Rev. B*, 97:201117, May 2018.
- [48] Aleksii Julku, Georg M. Bruun, and Päivi Törmä. Excitations of a bose-einstein condensate and the quantum geometry of a flat band. *Phys. Rev. B*, 104:144507, Oct 2021.
- [49] J Cayssol and J N Fuchs. Topological and geometrical aspects of band theory. *Journal of Physics: Materials*, 4(3):034007, apr 2021.
- [50] Alexander Kruchkov. Quantum geometry, flat chern bands, and wannier orbital quantization. *Phys. Rev. B*, 105:L241102, Jun 2022.
- [51] Kukka-Emilia Huhtinen, Jonah Herzog-Arbeitman, Aaron Chew, Bogdan A. Bernevig, and Päivi Törmä. Revisiting flat band superconductivity: Dependence on minimal quantum metric and band touchings. *Phys. Rev. B*, 106:014518, Jul 2022.
- [52] Tomoki Ozawa and Nathan Goldman. Probing localization and quantum geometry by spectroscopy. *Phys. Rev. Research*, 1:032019, Nov 2019.
- [53] Ingemar Bengtsson and Karol Zyczkowski. *Geometry of Quantum States: An Introduction to Quantum Entanglement*. Cambridge University Press, 2006.
- [54] Ran Cheng. Quantum geometric tensor (fubini-study metric) in simple quantum system: A pedagogical introduction. 2010.
- [55] Sebastiano Peotta and Päivi Törmä. Superfluidity in topologically nontrivial flat bands. *Nature Communications*, 6(1):8944, Nov 2015.
- [56] Aleksii Julku, Sebastiano Peotta, Tuomas I. Vanhala, Dong-Hee Kim, and Päivi Törmä. Geometric origin of superfluidity in the lieb-lattice flat band. *Phys. Rev. Lett.*, 117:045303, Jul 2016.
- [57] Murad Tovmasyan, Sebastiano Peotta, Päivi Törmä, and Sebastian D. Huber. Effective theory and emergent SU(2) symmetry in the flat bands of attractive hubbard models. *Phys. Rev. B*, 94:245149, Dec 2016.
- [58] Fang Xie, Zhida Song, Biao Lian, and B. Andrei Bernevig. Topology-bounded superfluid weight in twisted bilayer graphene. *Phys. Rev. Lett.*, 124:167002, Apr 2020.
- [59] Jonah Herzog-Arbeitman, Valerio Peri, Frank Schindler, Sebastian D. Huber, and B. Andrei Bernevig. Superfluid weight bounds from symmetry and quantum geometry in flat bands. *Phys. Rev. Lett.*, 128:087002, Feb 2022.
- [60] Jonah Herzog-Arbeitman, Aaron Chew, Kukka-Emilia Huhtinen, Päivi Törmä, and B. Andrei Bernevig. Many-body superconductivity in topological flat bands. 2022.